




CZTSSe thin films fabricated by single step deposition for superstrate solar cell applications

M. Terlemezoglu^{1,2,3} · Ö. Bayraklı Sürücü^{2,4} · C. Dogru^{1,2} · H. H. Güllü⁵ · E. H. Ciftpinar^{1,2} · Ç. Erçelebi^{1,2} · M. Parlak^{1,2} 

Received: 13 February 2019 / Accepted: 6 May 2019 / Published online: 13 May 2019
© Springer Science+Business Media, LLC, part of Springer Nature 2019

Abstract

The focus of this study is the characterization of $\text{Cu}_2\text{ZnSn}(\text{S},\text{Se})_4$ (CZTSSe) thin films and fabrication of CZTSSe solar cell in superstrate configuration. In this work, superstrate-type configuration of glass/ITO/CdS/CZTSSe/Au was entirely fabricated by totally vacuum-based process. CZTSSe absorber layers were grown by RF magnetron sputtering technique using stacked layer procedure. SnS, CuSe and ZnSe solid targets were used as precursors and no additional step like the selenization process was applied. The structural and morphological properties of deposited CZTSSe layers were analyzed using X-ray diffraction (XRD), Raman scattering, scanning electron microscopy (SEM) and energy dispersive X-ray spectroscopy analysis (EDS) measurements. The optical and electrical properties of the CZTSSe thin films were investigated by UV–Vis spectroscopy, Hall-Effect and photoconductivity measurements. In addition, the device performance of the fabricated superstrate solar cell was examined.

1 Introduction

Copper-zinc-tin-sulfo selenide $\text{Cu}_2\text{ZnSn}(\text{S},\text{Se})_4$ (CZTSSe) semiconductor has attracted more attention in recent years due to the similarity of its crystal structure with $\text{Cu}(\text{In},\text{Ga})\text{Se}_2$ (CIGSe) as well as its earth-abundant, low-cost constituent elements [1, 2]. CZTSSe is considered as a promising absorber material with its high absorption coefficient above 10^4 cm^{-1} , tunable direct band gap and p-type conductivity [3, 4]. Commonly, CZTSSe thin film based solar cells are fabricated in substrate configuration with a hole collecting molybdenum (Mo) back contact, which is the well-known configuration of CIGS technology [5]. However, the reported conversion efficiencies of CZTSSe based solar cells

are much lower than those of CIGSe based ones, so far [6]. Various techniques have been applied to deposit CZTSSe thin film layer such as sputtering [7, 8], thermal evaporation [9–11], electrodeposition [12], sol–gel [13], spray pyrolysis [14] and hydrazine-based solution method [15]. The current highest cell efficiency of CZTSSe based solar cell was reported as 12.6% using hydrazine-based solution method, which is not suitable for large-scale production since hydrazine is an extremely toxic and reactive chemical [15, 16]. On the other hand, reported power conversion efficiencies utilizing other production methods remain below 10%. The gap between the performance of CIGS and CZTSSe based solar cells could be related to some interface problems such as the aggressive reaction between the CZTSSe absorber layer and Mo back contact layer during thermal processing [5]. This leads to an undesirable Schottky barrier at the CZTSSe/Mo interface [16, 17]. High interface recombination and high series resistance have been reported as other problems limiting the device performance [1, 18]. Considering the high efficient CdTe solar cells in superstrate configuration, it is believed that superstrate configuration can be used to tackle some of the above mentioned problems of CZTSSe solar cells [16]. When compared with substrate configuration, superstrate configuration has several potential advantages such as reduction in material consumption and process time since it requires thinner window and absorber layers. It also offers a more suitable way of construction of

✉ M. Parlak
parlak@metu.edu.tr

¹ Department of Physics, Middle East Technical University, 06800 Ankara, Turkey

² Center for Solar Energy Research and Applications, Middle East Technical University, 06800 Ankara, Turkey

³ Department of Physics, Tekirdağ Namık Kemal University, 59030 Tekirdağ, Turkey

⁴ Department of Physics, Kırşehir Ahi Evran University, 40200 Kırşehir, Turkey

⁵ Department of Electrical and Electronics Engineering, Atılım University, 06836 Ankara, Turkey

tandem cell applications [19, 20]. In addition, the focus of research related to kesterite solar cells has recently shifted to superstrate-type configuration [1, 5, 16, 21].

In this study, CZTSSe thin film based solar cells were fabricated in superstrate configuration. CZTSSe thin films were deposited by RF magnetron sputtering. Following the characterization of deposited CZTSSe thin films, device characterization of CZTSSe based solar cells was carried out. As a result, fabricated CZTSSe based solar cell exhibited illumination photo response with $V_{oc} = 77$ mV, $J_{sc} = 2.45$ mA/cm².

2 Experimental details

In this study, The CZTSSe based solar cells were prepared in superstrate-type architecture utilizing indium tin oxide (ITO) coated glass substrates with the sheet resistivity of 10 Ω /sq. Before the cadmium sulfide (CdS) deposition, ITO coated glass substrates were subjected to a sequence of ultrasonic cleaning steps (acetone, isopropanol and DI water for 10 min. each). Subsequently, samples were dried in N₂ atmosphere. CdS layers were deposited on ITO coated glass substrates at room temperature using thermal evaporation with CdS (99.99%) powder as the source material. The base pressure of the evaporation chamber was about 5×10^{-6} Torr during the deposition and the thickness of CdS layers was about 100 nm. Then, SnS, CuSe and ZnSe precursor layers for CZTSSe were deposited on both glass substrate and CdS/ITO/glass using RF magnetron sputtering technique. CZTSSe/glass samples were used for material the characterization of deposited CZTSSe films. The RF power applied for SnS (99.99%), CuSe (99.99%) and ZnSe (99.99%) targets was 80 W in a typical sputtering run. The optimized deposition order was determined as SnS/CuSe/ZnSe/SnS/CuSe/ZnSe/SnS stacked layers in order to eliminate the metallic behavior on the top surface of film. The substrate temperature was kept at 150 °C and the chamber pressure was nearly 6×10^{-3} Torr during the deposition of precursors under 6 sccm Ar flow. After the deposition process, samples were subjected to post-annealing at 350 °C under N₂ atmosphere for 30 min. Then, Au was thermally evaporated as a back contact using Cu hard masks with dots of 500 μ m radius.

To investigate the morphological and compositional properties of deposited films, Quanta 400 FEG model scanning electron microscopy (SEM) equipped with energy dispersive X-ray spectroscopy analysis (EDS) system were used. The X-ray diffraction (XRD) measurements were performed using a Rigaku Miniflex XRD system equipped with a CuK α radiation source. Raman scattering measurements were carried out by using a Horiba-Jobin–Yvon iHR550 imaging spectrometer with the three-grating monochromators and a laser with the wavelength of 532 nm used as an excitation source. Dektak 6 M profilometer was used to measure the

thickness of thin film layer. The optical characterization of the CZTSSe thin film on glass substrate was performed by Perkin-Elmer Lambda 45 spectrophotometer. Hall-effect measurement was carried out to determine the electrical properties of the film by using Nanomagnetic Hall Effect system at a magnetic field strength of 0.9 T. In addition, temperature dependent conductivity measurements in the temperature range of 100–340 K were performed by using different illumination intensity in between 20 and 115 mW/cm² with the help of a Janis liquid nitrogen cryostat and Lake-Shore 331 temperature controller. External quantum efficiency (EQE) measurement of the CZTSSe solar cell were carried out by Bentham PVE 300 system. The current–voltage characteristics of the device were measured using computer controlled Keithley 2400 sourcemeter under dark and illumination of an AM 1.5 global spectrum.

3 Results and discussion

The chemical composition of the absorber film layer was determined by EDS analysis and the obtained spectrum showed characteristic peaks associated with the constituent elements without any impurity content. The relative atomic percentage of the elements in the deposited thin film was found as Cu:Zn:Sn:S:Se = 20:11:18:25:26%, which indicates that absorber layer has in Sn-rich behavior. The crystalline nature of this film layer was investigated performing XRD and Raman scattering measurements. The XRD profile of the CZTSSe thin film was given in Fig. 1a. In this figure, three diffraction peaks around angles of 27.9, 46.1 and 54.6 were observed and these reflections of X-rays were associated with the crystalline orientations in the plane directions of (112), (220) and (312) in a good agreement with kesterite CZTSSe structure, respectively (ICDD data #00-052-0868 CZTSe and ICDD data#00-026-0575 CZTS). The Miller indices associated with peaks were also given in the figure. XRD pattern of CdS layer was also given in the inset of Fig. 1a. It has polycrystalline structure and the predominant diffraction peak at $2\theta = 26.2^\circ$ was indexed as (111) plane, corresponding to the hexagonal wurtzite phase of CdS. The crystalline phase identification and also complemented analysis the existence of possible secondary phases in the CZTSSe structure was performed by Raman scattering measurements. In literature, the dominant Raman peaks at 196 and 338 cm⁻¹ correspond to A₁ modes of the CZTSe and CZTS structures, respectively [4, 22]. As shown in Fig. 1b, the detected peaks at 198 cm⁻¹ and 328 cm⁻¹ could be evaluated as being A₁ mode frequencies of the CZTSSe structure. It can be the fact that the shift of A₁ vibration modes is observed in the Raman spectrum of CZTSSe structure due to the substitution of S by Se. The additional Raman peak found at 240 cm⁻¹ is well-matched with the elementary Se

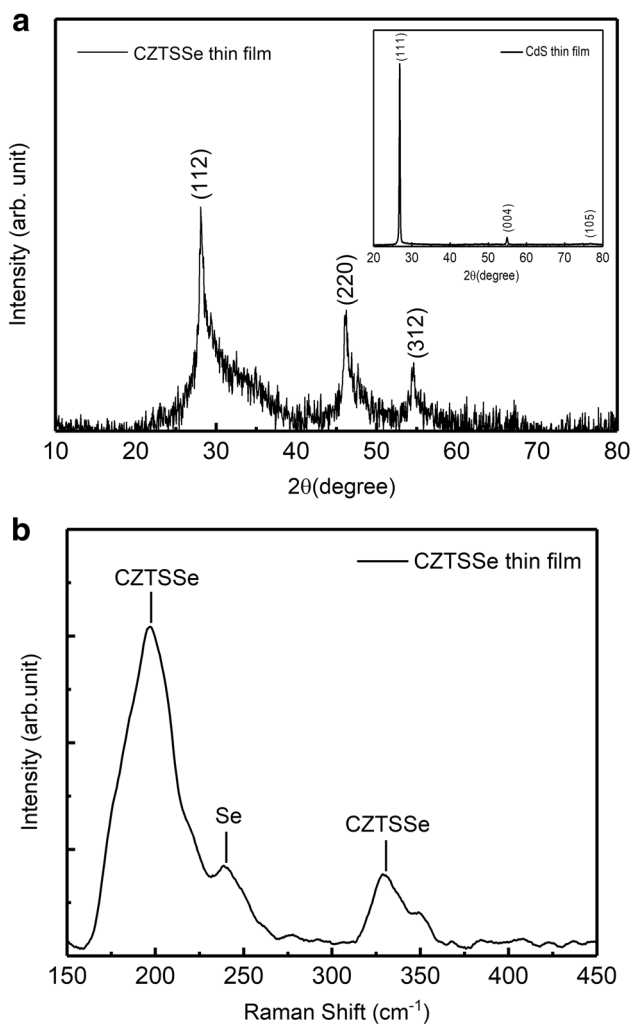


Fig. 1 **a** The XRD pattern of CZTSSe layer (inset shows the XRD pattern of CdS layer), **b** Raman spectrum of CZTSSe layer

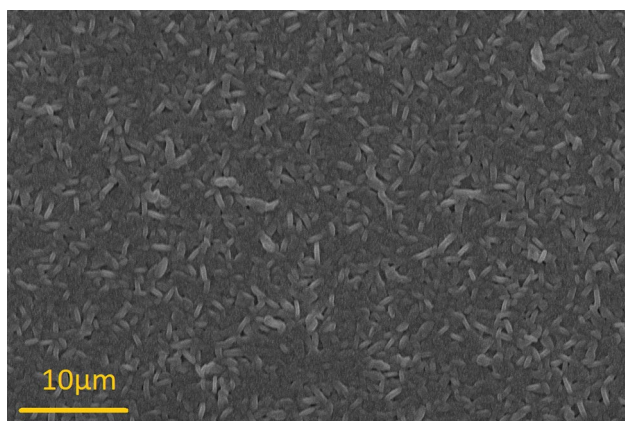


Fig. 2 The SEM surface image of CZTSSe thin film

contribution to the structure [11]. On the other hand, there is no another Raman peak originated by binary or ternary phases in the deposited CZTSSe film. The surface morphology of the CZTSSe thin film was observed utilizing SEM measurement. The obtained top-view SEM image of the sample surface indicates a series of close-packed CZTSSe grains without any void on the surface of the film (Fig. 2). This result can be the indication of well-deposited film surface that positively affects getting solar cell having better device parameters. The optical characteristics of the film layer were investigated by transmittance (T) and reflectance (R) measurements performed at room temperature. In the region of interest for photovoltaic applications, the film showed a very low optical transmittance below 5% and a reflectance of about 15% as presented in Fig. 3a. Based on these experimental results, the absorption coefficient (α) values were calculated by using the following equation,

$$T = (1 - R)^2 e^{-\alpha t} \tag{1}$$

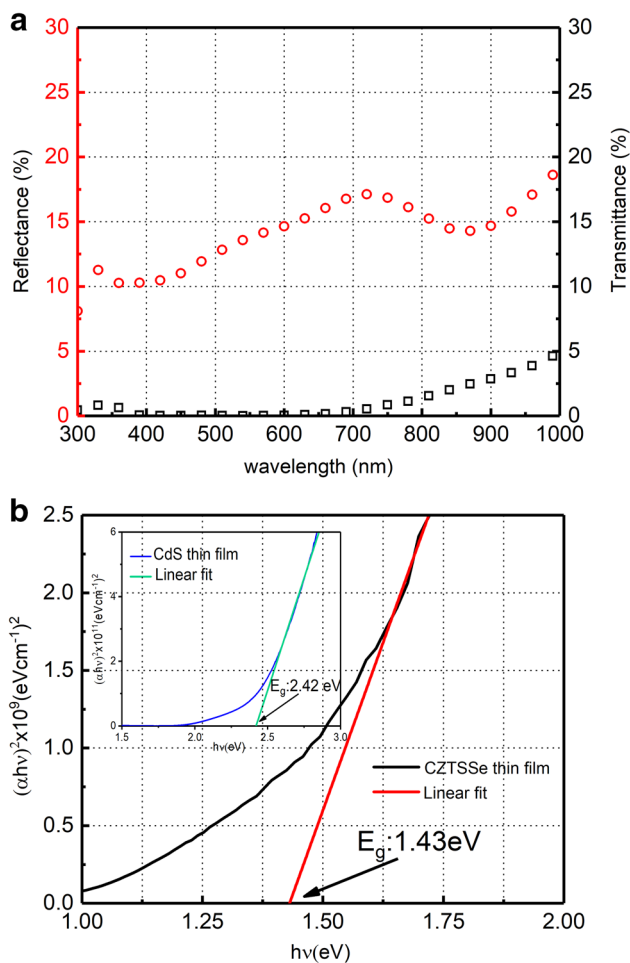


Fig. 3 **a** The plot of transmittance and reflectance as a function of wavelength, **b** $(\alpha h\nu)^2$ vs $h\nu$ graph for CZTSSe thin film. (Inset shows the $(\alpha h\nu)^2$ vs $h\nu$ graph for CdS layer)

where t is the thickness of the film layer. The α values were found above 10^4 cm^{-1} in the visible and near-IR region which are in a good agreement with the properties of the CZTSSe absorber films reported in the literature [23]. According to the direct optical transition behavior, the optical band gap of the film was calculated by Tauc relation,

$$(\alpha hv) = A(hv - E_g)^{1/2} \quad (2)$$

where A is constant, hv is the incident photon energy, E_g is the optical band gap [24]. In the Tauc plot given in Fig. 3b, E_g value was found by extrapolating the linear part to the energy axis. As a result of linear fitting process, the gap value was determined as about 1.43 eV, which is well-consistent with the reported values for CZTSSe [22, 23]. Furthermore, the direct band gap value of the CdS layer was found to be 2.42 eV given in the inset of Fig. 3b.

The electrical properties of the CZTSSe thin film structure were investigated by room temperature Hall-effect and temperature dependent conductivity measurements on the film layer deposited in Van der Pauw geometry and prepared with Au front metal contact evaporation through suitable contact geometry. The room temperature resistivity value was extracted as $0.57 \text{ } \Omega \cdot \text{cm}$ according to the standard technique of four-contact van der Pauw method. As a result of Hall-effect measurement, CZTSSe film was found in p-type semiconductor behavior from the sign of Hall voltage. In addition, carrier concentration and mobility of the sample were obtained as $3.93 \times 10^{18} \text{ cm}^{-3}$ and $2.77 \text{ cm}^2/\text{V}\cdot\text{s}$, respectively. The temperature variations in the dark conductivity (σ) values were shown in Fig. 4. This conductivity profile of CZTSSe thin film indicates Arrhenius behavior which is an increasing exponential variation with increasing

temperature. This observed temperature dependent behavior was modeled according to the following expression as [25],

$$\sigma_T = \sigma_{0T} \exp\left(-\frac{E_a}{k_B T}\right) \quad (3)$$

where σ_{0T} is the pre-exponential term, T is the ambient temperature, k_B is the Boltzmann constant and E_a is the activation energy based on thermionic emission model. In this analysis, the activation energies were calculated from the relation between $\ln(\sigma)$ and $1000/T$ and three linear regions with E_a values of 9.7 meV for 250–340 K, 2.8 meV for 150–200 K and 0.7 meV for 100–140 K regions were obtained as inferred from the linear lines in the inset of Fig. 4. These energy values can be related to the existence of possible shallow trap centers in the structure that can take part in the conduction process at specific temperature intervals [26, 27]. In addition, the photoconductivity values were observed higher than the values in dark condition at each illumination intensity and temperature step due to the current contribution of excited carriers under illumination. As given in Fig. 4, it was found that, at each temperature, the conductivity with the photo-excited carriers are directly proportional to the illumination intensity and at each illumination, contribution to the conductivity also increases exponentially with increase in temperature [28].

The photovoltaic performance of CZTSSe based solar cell in superstrate configuration was evaluated under irradiation of AM 1.5. The current–voltage curves under dark and illumination are given in Fig. 5. This configuration could be illuminated from either side. Illumination of the solar cell from the glass was labeled as primary illumination while illumination from back side of the solar cell was labeled as the secondary illumination. The main solar cell parameters were obtained from the primary

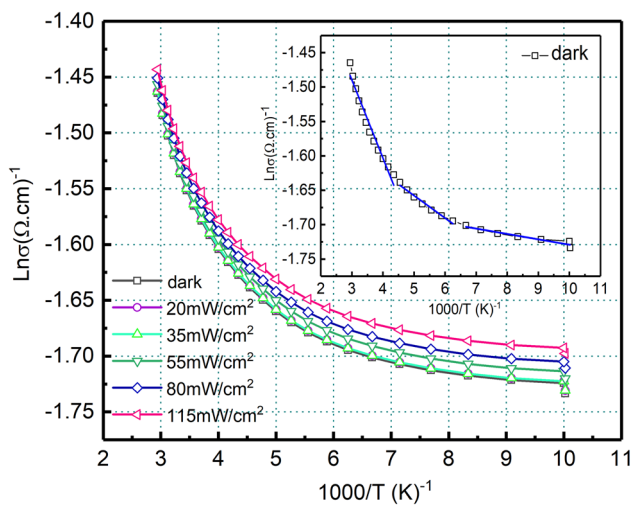


Fig. 4 Temperature dependent dark and illuminated conductivity behavior of CZTSSe thin film layer. The inset shows the variation of dark conductivity

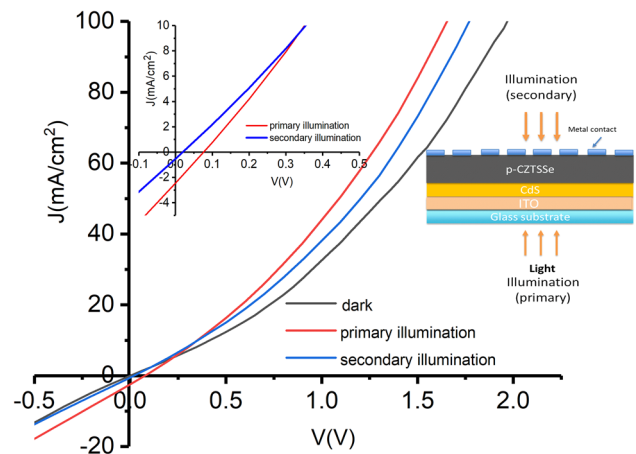


Fig. 5 J-V graph for ITO/CdS/CZTSSe/Au solar cell under dark and illumination. Inset shows the J-V graph of the solar cell at the voltage range of 0 and 0.5 V

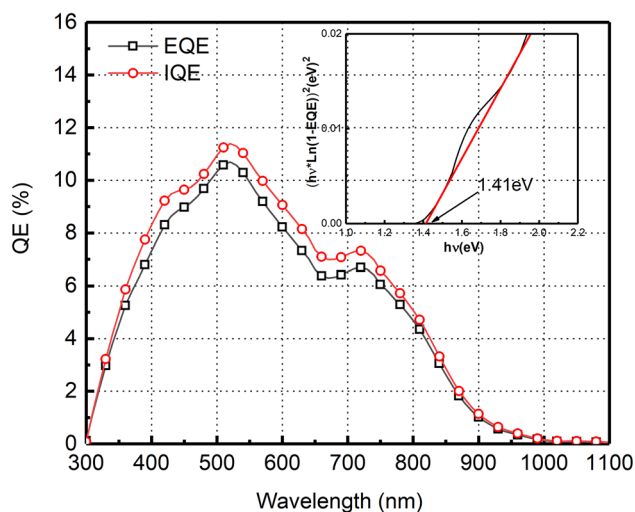


Fig. 6 External quantum efficiency (EQE) spectrum of ITO/CdS/CZTSSe/Au structure. The inset shows the $[\hbar\nu \cdot \ln(1 - EQE)]^2$ vs $\hbar\nu$ plot of CZTSSe layer

illumination. The power conversion efficiency was about 0.1% with a short-circuit density (J_{sc}) of 2.45 mA cm^{-2} , open circuit voltage (V_{oc}) of 77 mV and fill factor (FF) of 25%. V_{oc} value is much lower than of superstrate type kesterite solar cells in the literature. Under illumination, the series resistance (R_s) and shunt resistance (R_{sh}) were found as $16 \Omega \text{ cm}^2$ and $101 \Omega \text{ cm}^2$, respectively. The series resistance value is much higher than the obtained value in the literature [1, 5, 21]. The key limiting factor in the efficiency of the CZTSSe solar cell is high R_s and low V_{oc} values, which is attributed to the poor quality of the film, interface recombination and some contact problems. In addition, low-response to illumination was observed when the solar cell was illuminated from the contact side (secondary illumination), as observed from Fig. 5. The external quantum efficiency (EQE) of CZTSSe solar cell as a function of wavelength was measured and the result is given in Fig. 6. Moreover, internal quantum efficiency was calculated by using the following expression,

$$IQE = \frac{EQE}{1 - R} \quad (4)$$

The maximum value of EQE was found as 11% almost at 500 nm which could be attributed to optical absorption of CdS. Then, the signals decayed abruptly. The short circuit current (J_{sc}) was calculated 2.3 mA/cm^2 from the external quantum efficiency measurement, which is in good agreement with the value of J_{sc} obtained from the current–voltage measurement. In addition, the extrapolation to zero of linear fitting in the plot of $[\hbar\nu \cdot \ln(1 - EQE)]^2$ versus $\hbar\nu$ gives the band gap energy of CZTSSe at 1.41 eV (inset of Fig. 6).

4 Conclusion

In this study, CZTSSe thin films were deposited using RF magnetron sputtering in which SnS, CuSe and ZnSe binary compounds were used as precursors. The XRD and Raman spectroscopic analyses indicated the presence of CZTSSe compound and no trace of secondary phases detected except for elementary Se peak. EDS analysis showed Sn-rich composition in the deposited films. Band gap energy was calculated as 1.43 eV with the help of transmittance and reflectance measurements. Then, using the optimized CZTSSe absorber layer, CZTSSe based solar cells were fabricated in superstrate configuration. The solar cell performance of ITO/CdS/CZTSSe/Au structure was discussed using the results of current–voltage measurements under dark and illumination with 100 mW/cm^2 and quantum efficiency measurement. The best cell efficiency was nearly 0.1% with $V_{oc} = 77 \text{ mV}$, $J_{sc} = 2.45 \text{ mA/cm}^2$.

Acknowledgement This work was financed by Middle East Technical University BAP under Grant No. GAP-105-2018-2755.

References

1. M. Berruet, Y. Di Iorio, C.J. Pereyra, R.E. Marotti, M. Vázquez, Phys. Status Solidi **11**(8), 1700144 (2017)
2. C. Yan, K. Sun, F. Liu, J. Huang, F. Zhou, X. Hao, Sol. Energy Mater. Sol. Cells **160**, 7 (2017)
3. J. He, L. Sun, S. Chen, Y. Chen, P. Yang, J. Chu, J. Alloys Compd. **511**, 129 (2012)
4. M. Grossberg, J. Krustok, J. Raudoja, K. Timmo, M. Altsaar, T. Raadik, Thin Solid Films **519**, 7403 (2011)
5. Y. Zhang, Y. Sun, H. Wang, H. Yan, Phys. Status Solidi **213**, 1324 (2016)
6. J. He, L. Sun, N. Ding, H. Kong, S. Zuo, S. Chen, Y. Chen, P. Yang, J. Chu, J. Alloys Compd. **529**, 34 (2012)
7. D.H. Son, D.H. Kim, S.N. Park, K.J. Yang, D. Nam, H. Cheong, J.K. Kang, Chem. Mater. **27**, 5180 (2015)
8. N. Ryota, T. Kunihiro, U. Hisao, J. Kazuo, W. Tsukasa, K. Hironori, Jpn. J. Appl. Phys. **53**(2S), 02BC10 (2014)
9. K. Oishi, G. Saito, K. Ebina, M. Nagahashi, K. Jimbo, W.S. Maw, H. Katagiri, M. Yamazaki, H. Araki, A. Takeuchi, Thin Solid Films **517**, 1449 (2008)
10. B. Shin, O. Gunawan, Y. Zhu, N.A. Bojarczuk, S.J. Chey, S. Guha, Prog. Photovoltaics Res. Appl. **21**, 72 (2013)
11. Ö. Bayraklı, M. Terlemezoğlu, H.H. Güllü, M. Parlak, Mater. Res. Express **4**, 086411 (2017)
12. J. Li, T. Ma, M. Wei, W. Liu, G. Jiang, C. Zhu, Appl. Surf. Sci. **258**, 6261 (2012)
13. F. Yakuphanoglu, Sol. Energy **85**, 2518 (2011)
14. N. Kamoun, H. Bouzouita, B. Rezig, Thin Solid Films **515**, 5949 (2007)
15. W. Wang, M.T. Winkler, O. Gunawan, T. Gokmen, T.K. Todorov, Y. Zhu, D.B. Mitzi, Adv. Energy Mater. **4**, 1301465 (2014)
16. C.-L. Wang, C.-C. Wang, B. Reeja-Jayan, A. Manthiram, RSC Adv. **3**, 19946 (2013)

17. O. Gunawan, T.K. Todorov, D.B. Mitzi, *Appl. Phys. Lett.* **97**, 233506 (2010)
18. D.B. Mitzi, O. Gunawan, T.K. Todorov, D.A.R. Barkhouse, *Philos. Trans. A. Math. Phys. Eng. Sci.* **371**, 20110432 (2013)
19. P. Xin, J.K. Larsen, F. Deng, W.N. Shafarman, *Sol. Energy Mater. Sol. Cells* **157**, 85 (2016)
20. M.D. Heinemann, F. Ruske, D. Greiner, A.R. Jeong, M. Rusu, B. Rech, R. Schlatmann, C.A. Kaufmann, *Sol. Energy Mater. Sol. Cells* **150**, 76 (2016)
21. D. Lee, K. Yong, *Nanotechnology* **25**, 065401 (2014)
22. M. Terlemezoglu, Ö. Bayraklı, H.H. Güllü, T. Çolakoğlu, D.E. Yıldız, M. Parlak, *J. Mater. Sci.* **29**, 5264 (2018)
23. Z. Shi, D. Attygalle, A.H. Jayatissa, *J. Mater. Sci.: Mater. Electron.* **28**, 2290 (2017)
24. N.M. Shinde, D.P. Dubal, D.S. Dhawale, C.D. Lokhande, J.H. Kim, J.H. Moon, *Mater. Res. Bull.* **47**, 302 (2012)
25. H.H. Güllü, M. Terlemezoglu, Ö. Bayraklı, D.E. Yıldız, M. Parlak, *Can. J. Phys.* **96**, 816 (2018)
26. J.Y.W. Seto, *J. Appl. Phys.* **46**, 5247 (1975)
27. N.F. Mott, E.A. Davis, *Electronic Processes in Non-Crystalline Materials* (Clarendon Press, Oxford, 1979)
28. R.H. Bube, *Photoelectronic Properties of Semiconductors* (Cambridge University Press, Cambridge, 1992)

Publisher's Note Springer Nature remains neutral with regard to jurisdictional claims in published maps and institutional affiliations.